ENTROPY ANALYSIS IN CILIATED INCLINED CHANNEL FILLED WITH HYDROMAGNETIC WILLIAMSON FLUID-FLOW INDUCED BY METACHRONAL WAVES

by

Najma SALEEM *

Department of Mathematics and Natural Sciences,
Prince Mohammad Bin Fahd University, Khobar, Saudi Arabia

Original scientific paper
https://doi.org/10.2298/TSCI191006183S

This study reveals the entropy analysis of hydromagnetic pumping flow of Williamson fluid through a 2-D symmetric channel carrying cilia. Propulsive metachronal waves are mobilized by whipping and beating of uniformly distributed cilia which follow elliptic trajectory movements in the parallel direction of flow. The flow is resisted by a uniform transverse magnetic field. The entire study is carried out in wave frame of reference. After implying lubrication approximations, the governing equations of the present flow problem are solved by perturbation method. Effects of physical parameters of interest on various flow quantities, the total entropy generation number and the Bejan number are plotted and discussed. It is observed that fluid velocity and temperature is enhanced in the core channel region for small values of Hartmann number and cilia length. It is also noticed that the entropy generation and the Bejan number are decreasing function of magnetic field. Near the channel center, irreversibility due to fluid friction is dominant but at the channel wall heat transfer irreversibility effects are observed to be substantial. The confined bolus reduces in size for small values of cilia length parameter and large values of Hartmann number.

Key words: *entropy generation, inclined ciliated channel, Williamson fluid, magnetic field*

Introduction

Ciliated assisted propulsions play a vital role in many physiological and biological systems. Cilia look like protuberances, present on the outer side of eukaryotic cells. These are slender extensions of plasma membrane, sustained internally by microtubules of the cytoskeleton and measuring about 1-10 μm in length. These appendage organelles propel the fluid and suspended particles passing through the surface. Cilia are smaller in size than flagella but frequent in numbers. They tend to move in a group and create a wave effect. Cilia are divided into two main groups named motile cilia and primary cilia. Motile cilia are present in respiratory system [1, 2] where they support to breathe smoothly without irritation make airways clear by preventing mucus and dust, lining of the female fallopian tube [3, 4] where they help in fertilization and also are responsible for moving the eggs towards uterus, male efferent ductules [5] where they mix the sperms to keep them from accumulating and hindering the tube so they can reach to their decisive endpoint. They also help in the movement of spinal fluid through the

* Author's e-mail: nsaleem@pmu.edu.sa

brain. Primary cilia work as sensory apparatus for the cell [6] and play an essential role in sensory neurons. They are found in kidneys, eye retina, ears and brains. Due to its diverse applications in human life, it has become an appealing field of research for many researchers. Brennen [7] investigated the locomotion of cell through a viscous fluid induced by a harmonic wave of progression on its surface. Qiu *et al.* [8] have reported that in order to move many biological microorganisms, cilia and flagella perform mutual movements (at low Reynolds number) by assuming non-Newtonian fluids as medium that carry shear thinning and shear thickening effects. Eytan and Elad [9] have reported a theoretical study of transport of egg in the fallopian tube and ovum in the uterine cavity by supposing that intra uterine fluid motion is primarily intended due to myometrial contractions. Recently, Farooq *et al.* [10] have investigated the flow of non-Newtonian fluid in a symmetric channel. It is assumed that the flow is induced by metachronal waves of progression of cilia whips reside on the inner side of the channel wall under lubrication approximations. Farooq and Siddiqui [11] explored the transport of seminal fluid through the ductus efferent due to metachronal propulsions of cilia beats in couple stress fluid. The involvement of cilia in the female fallopian tube and uterus are reported in some recent studies of [12, 13].

Most of the biological fluids (such as blood, plasma and liquid metals, *etc.*), due to their composition are considered as hydromagnetic fluids. The mutual interaction of fluid motion and magnetic field has found wide applications in physiology and engineering. Stud *et al.* [14] investigated the influence of moving magnetic field on the blood flow and reported that it augmented the fluid-flow. Maqbool *et al.* [15] have studied the MHD flow of Jeffery fluid induced due to cilia beats. Hayat *et al.* [16] have investigated the influence of magnetic field on Carreau fluid-flow in symmetric channel and reported that large value of Hartman number boosts the axial velocity at the channel wall but its behavior is quite opposite at the channel center. Peristaltic transport of Williamson fluid through micro-channel in the presence of an applied external magnetic field was investigated by Parkesh *et al.* [17]. Many researchers [18, 19] have studied the effects of external magnetic field on peristaltic motion of non-Newtonian fluid as blood under different conditions.

In order to produce energy in human body, metabolism is a significant mechanism. Human body is accepted to be more highly ordered as compared to non-living objects. But this does not oppose the Second law of thermodynamics. In order to maintain life, humans absorb the food and expel the disordered waste materials in the form of CO_2, urine, breath, and feces. This increases the overall entropy of the system and may affects blood-flow, urine movement, and food absorption, *etc.* Another type of metabolism termed as catabolism is the breakdown of the complex molecules into small molecules to produce energy. Human body extracts the chemical energy in the food and uses it to sustain or reduce the local entropy levels thus to conserves life. The Second law of thermodynamics accompanied by the entropy mechanism also has high significance in this process. The pioneer work reporting entropy generation in four different types of heat convection process was presented by Bejan [20]. Bejan [21] reported that how the overall entropy of a thermal system can be minimized by optimize thermal efficient system. Moreover, it was revealed that the heat transfer and the viscous dissipation are two main sources of entropy production in the system. After this innovative work of Bejan, many researchers [22-24] investigated the phenomenon of entropy in connective heat transfer processes under various assumptions. However, a very few studies have been conducted for entropy analysis in biological systems. In this regard, Souidi *et al.* [25] described the entropy production effects on peristaltic pump in a contracting tube. Akbar [26] examined the entropy production in MHD peristaltic flow inside a tube. Munawar *et al.* [27] investigated the second-law analysis in a peristaltic flow of variable viscosity fluid and revealed that entropy production is high in the contracted region and reduces in the wider channel part. Recently, Saleem [28] observed the entropy production in blood flow through an asymmetric channel.

The aforementioned literature sheds light on the importance of entropy analysis in biological fluids. However still there is a room for studying the second law in ciliated channel. This instigates us to examine the entropy analysis of MHD flow of Williamson fluid through an inclined ciliated symmetric channel. It is assumed that the flow is induced due to metachronal strokes of cilia that generate rhythmic waves at the channel wall. Heat transfer and fluid friction irreversibilities are anticipated to be the main causes of entropy production. The governing equations are modeled and simplified under the assumptions of long wavelength and low Reynolds number. The analytic series solution are obtained using perturbation technique and result are compared with a numerical shooting method. Flow and heat transfer quantities are calculated, and the analysis is carried out by providing graphical illustrations.

Mathematical formulation

Consider 2-D MHD pumping flow of an incompressible Williamson fluid through an inclined symmetric channel lining small hair like structures (cilia) that stripe inside the channel wall surface under the effects of constant magnetic field and heat transfer. It is also assumed that the flow is induced due to rhythmic beatings of cilia (with constant speed c) that synchronize their beats to set metachronal waves pattern along the channel boundaries, fig. 1. Using a rectangular co-ordinate system, X-axis is taken along the direction of wave propagation and Y-axis normal to it. The configuration of ciliated wall in laboratory frame is defined:

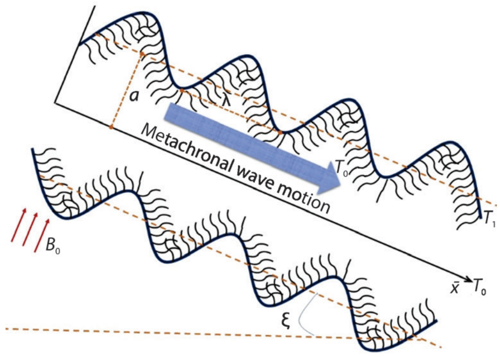

Figure 1. The schematic diagram of the ciliated inclined channel

$$Y = \eta\left(\bar{X}, t\right) = H = \left\{ a + a\varepsilon \cos\left[\frac{2\pi}{\lambda}\left(\bar{X} - ct\right)\right]\right\} \tag{1}$$

It is assumed that cilia tips move by following elliptical motion pattern and are vertically located:

$$\bar{X} = \phi\left(\bar{X}, t\right) = X_0 + a\varepsilon\alpha \sin\left[\frac{2\pi}{\lambda}\left(\bar{X} - ct\right)\right] \tag{2}$$

where a, α, ε, H, t, λ, and X_0 are mean channel width, eccentricity of elliptic path, cilia length parameter, half channel width, time, wavelength and indicated position of the particle.

In laboratory frame the axial and transverse velocity components at channel boundaries and governing equations of present flow problem are written [29, 30]:

$$U_0 = \left(\frac{\partial \bar{X}}{\partial t}\right)_{X_0} = \frac{-\left(\dfrac{2\pi}{\lambda}\right) ac\varepsilon\alpha \cos\left[\dfrac{2\pi}{\lambda}\left(\bar{X} - ct\right)\right]}{1 - \left(\dfrac{2\pi}{\lambda}\right) a\varepsilon\alpha \cos\left[\dfrac{2\pi}{\lambda}\left(\bar{X} - ct\right)\right]} \tag{3}$$

$$V_0 = \left(\frac{\partial \bar{Y}}{\partial t}\right)_{X_0} = \frac{-\left(\frac{2\pi}{\lambda}\right) ac\varepsilon\alpha\cos\left[\frac{2\pi}{\lambda}\left(\bar{X}-ct\right)\right]}{1-\left(\frac{2\pi}{\lambda}\right) a\varepsilon\alpha\cos\left[\frac{2\pi}{\lambda}\left(\bar{X}-ct\right)\right]} \tag{4}$$

$$\frac{\partial \bar{U}}{\partial \bar{X}} + \frac{\partial \bar{V}}{\partial \bar{Y}} = 0 \tag{5}$$

$$\rho\left(\frac{\partial}{\partial t} + \bar{U}\frac{\partial}{\partial \bar{X}} + \bar{V}\frac{\partial}{\partial \bar{Y}}\right)\bar{U} = -\frac{\partial \bar{P}}{\partial \bar{X}} + \frac{\partial \bar{S}_{\bar{X}\bar{X}}}{\partial \bar{X}} + \frac{\partial \bar{S}_{\bar{X}\bar{Y}}}{\partial \bar{Y}} - \sigma B_0^2 \bar{U} + \rho g\sin\left(\xi\right) \tag{6}$$

$$\rho\left(\frac{\partial}{\partial t} + \bar{U}\frac{\partial}{\partial \bar{X}} + \bar{V}\frac{\partial}{\partial \bar{Y}}\right)\bar{V} = -\frac{\partial \bar{P}}{\partial \bar{Y}} + \frac{\partial \bar{S}_{\bar{X}\bar{Y}}}{\partial \bar{X}} + \frac{\partial \bar{S}_{\bar{Y}\bar{Y}}}{\partial \bar{Y}} - \rho \mathrm{g}\cos\left(\xi\right) \tag{7}$$

$$\rho\zeta\left(\frac{\partial}{\partial t} + \bar{U}\frac{\partial}{\partial \bar{X}} + \bar{V}\frac{\partial}{\partial \bar{Y}}\right)\bar{T} = \kappa\left(\frac{\partial^2 \bar{T}}{\partial \bar{X}^2} + \frac{\partial^2 \bar{T}}{\partial \bar{Y}^2}\right) + \bar{S}_{\bar{X}\bar{X}}\frac{\partial \bar{U}}{\partial \bar{X}} + \bar{S}_{\bar{X}\bar{Y}}\left(\frac{\partial \bar{U}}{\partial \bar{Y}} + \frac{\partial \bar{V}}{\partial \bar{X}}\right) + \bar{S}_{\bar{Y}\bar{Y}}\frac{\partial \bar{V}}{\partial \bar{Y}} \tag{8}$$

where P is the pressure, ρ – the electrical conductivity of the fluid, B_0 – the constant magnetic, ξ – the inclination angle, ζ – the specific heat at constant volume, κ – the thermal conductivity, and T – the fluid temperature. The extra stress components for the Williamson fluid are found:

$$\boldsymbol{S} = \left[\mu_\infty + \left(\mu_0 - \mu_\infty\right)\left(1 - \Gamma\bar{\dot{\gamma}}\right)^{-1}\right]\bar{\dot{\gamma}} \tag{9}$$

$$\bar{\dot{\gamma}} = \sqrt{\frac{1}{2}\sum_i\sum_j \bar{\dot{\gamma}}_{ij}\bar{\dot{\gamma}}_{ji}} = \sqrt{\frac{1}{2}\Pi} \tag{10}$$

where μ_∞, μ_0, Γ, and Π are the infinite shear rate viscosity, the zero-shear rate viscosity, the time constant and the second invariant strain tensor, respectively. By assuming $\mu_\infty = 0$ and $\Gamma\bar{\dot{\gamma}} < 1$ eq. (11) gives:

$$\bar{\mathbf{S}} = \mu_0\left(1 + \Gamma\bar{\dot{\gamma}}\right)\bar{\dot{\gamma}} \tag{11}$$

Defining the transformations for converting in wave frame $(\bar{x}, \bar{y})$ from the laboratory frame $(\bar{X}, \bar{Y})$:

$$\bar{x} = \bar{X} - ct,\ \bar{y} = \bar{Y},\ \bar{u} = \bar{U} - c,\ \bar{v} = \bar{V},\ \bar{p}\left(x, y\right) = \bar{P}\left(\bar{X}, \bar{Y}, t\right) \tag{12}$$

and introducing non-dimensional quantities:

$$x = \frac{\bar{x}}{\lambda},\ y = \frac{\bar{y}}{a},\ u = \frac{\bar{u}}{c},\ v = \frac{\lambda\bar{v}}{ac},\ \beta = \frac{a}{\lambda},\ H = \frac{\bar{H}}{a},\ t = \frac{c\bar{t}}{a},\ p = \frac{a^2\bar{p}}{\mu c\lambda}$$

$$\mathbf{S} = \frac{a}{\mu_0 c}\bar{\mathbf{S}},\ \mathrm{Re} = \frac{\rho ac}{\mu_0},\ \mathrm{We} = \frac{\Gamma c}{a},\ \mathrm{Fr} = \frac{c^2}{ga},\ \mathrm{M} = \sqrt{\frac{\sigma}{\mu_0}}B_0 a,\ \mathrm{Pr} = \frac{\rho\nu\zeta}{\kappa} \tag{13}$$

$$\theta = \frac{T - T_0}{T_1 - T_0},\ \mathrm{Ec} = \frac{c^2}{\zeta\left(T_1 - T_0\right)},\ \mathrm{Br} = \mathrm{EcPr}$$

where β is the wave number, Re – the Reynolds number, We – the Weissenberg number, Fr – the Froude number, M – the Hartmann number, Pr – the Prandtl number, Ec – the Eckert number, and Br – the Brinkman number.

Using eqs. (12) and (13) into eqs. (5)-(9) and after employing long wavelength and small wave number approximations:

$$\frac{\partial p}{\partial x}=\frac{\partial}{\partial y}\left[\frac{\partial u}{\partial y}+\mathrm{We}\left(\frac{\partial u}{\partial y}\right)^2\right]-\mathrm{M}^2u+\frac{\mathrm{Re}}{\mathrm{Fr}}\sin(\xi) \tag{14}$$

$$\frac{\partial p}{\partial y}=0 \tag{15}$$

$$\frac{\partial^2\theta}{\partial y^2}=-\mathrm{Br}\left[\left(\frac{\partial u}{\partial y}\right)^2+\mathrm{We}\left(\frac{\partial u}{\partial y}\right)^3\right] \tag{16}$$

The dimensionless boundary conditions of the flow problem are defined:

$$\frac{\partial u}{\partial y}=0,\ \frac{\partial\theta}{\partial y}=0\ \text{ at }\ y=0 \tag{17}$$

$$u=-1-\frac{2\pi\alpha\varepsilon\beta\cos(2\pi x)}{1-2\pi\alpha\varepsilon\beta\cos(2\pi x)},\ \theta=1\ \text{at}\ y=h=1+\varepsilon\cos(2\pi x) \tag{18}$$

The pressure per metachronal wavelength and dimensionless mean flow rate in the fixed, Q, and wave frame, F, are defined:

$$\Delta P_\lambda=\int_0^1\left(\frac{\mathrm{d}p}{\mathrm{d}x}\right)\mathrm{d}x,\ Q=1+F \tag{19}$$

The perturbation solution

In order to find the solution of eqs. (14) and (16) subject to the boundary conditions eqs. (17)-(18), we use perturbation technique by selecting We ($\ll$1) as perturbation parameter. Weissenberg number expand the flow quantities:

$$u=u_0+\mathrm{We}u_1+O\left(\mathrm{We}^2\right),\ \frac{\mathrm{d}p}{\mathrm{d}x}=\frac{\mathrm{d}p_0}{\mathrm{d}x}+\mathrm{We}\frac{\mathrm{d}p_1}{\mathrm{d}x}+O\left(\mathrm{We}^2\right)$$

$$\theta=\theta_0+\mathrm{We}\theta_1+O\left(\mathrm{We}^2\right),\ F=F_0+\mathrm{We}F_1+O\left(\mathrm{We}^2\right)$$

and get zeroth order and first order system of equations.

Zeroth order system

$$\frac{\partial p_0}{\partial x}=\frac{\partial^2u_0}{\partial y^2}-\mathrm{M}^2u_0+\frac{\mathrm{Re}}{\mathrm{Fr}}\sin(\xi) \tag{20}$$

$$\frac{\partial p_0}{\partial y}=0 \tag{21}$$

$$\frac{\partial^2\theta_0}{\partial y^2}=-\mathrm{Br}\left(\frac{\partial u_0}{\partial y}\right)^2 \tag{22}$$

$$\frac{\partial u_0}{\partial y}=0,\ \frac{\partial\theta_0}{\partial y}=0\ \text{ at }\ y=0 \tag{23}$$

$$u_0 = -1 - \frac{2\pi\varepsilon\alpha\beta\cos(2\pi x)}{1-2\pi\varepsilon\alpha\beta\cos(2\pi x)}, \ \theta_0 = 1 \ \text{at} \ y = h \tag{24}$$

First order system

$$\frac{\partial p_1}{\partial x} = \frac{\partial^2 u_1}{\partial y^2} + \frac{\partial}{\partial y}\left[\left(\frac{\partial u_0}{\partial y}\right)^2\right] - \mathrm{M}^2 u_1 \tag{25}$$

$$\frac{\partial p_1}{\partial y} = 0 \tag{26}$$

$$\frac{\partial^2 \theta_1}{\partial y^2} = -\mathrm{Br}\left[\left(\frac{\partial u_0}{\partial y}\right)^3 + 2\frac{\partial u_0}{\partial y}\frac{\partial u_1}{\partial y}\right] \tag{27}$$

$$\frac{\partial u_1}{\partial y} = 0, \ \frac{\partial \theta_1}{\partial y} = 0 \ \text{at} \ y = 0 \tag{28}$$

$$u_1 = 0, \ \theta_1 = 1 \ \text{at} \ y = h \tag{29}$$

The zeroth order and first order systems of equations are solved by using computational software MATHEMATICA. The data for pressure rise per metachronal wavelength is obtained by numerical integration of eq. (19). The perturbation series solution for the present problem has been verified by solving eqs. (14)-(18) numerically with shooting method. Table 1 is plotted to show the comparison of the numerical values of skin friction $u'(h)$. The table shows an adequate match between the perturbation and numerical results.

Table 1. Numerical data for skin friction at the ciliated channel wall obtained by analytical and numerical techniques when Q = 3, $\alpha = \varepsilon$ = 0.2, $\beta = x$ = 0.5, Fr = Re = 1, M = 0.5

We	$u'(h)$ (Perturbation)	$u'(h)$ (Numerical)
0	–12.8413	–12.8413
0.00001	–12.8326	–12.8382
0.0001	–12.7541	–12.8112
0.001	–12.4631	–12.5971
0.01	–11.7520	–11.8814

Entropy analysis

It is assumed that the entropy in cilia supported flow is produced due to heat transfer and fluid friction. By following [31-33], the equation of total volumetric local rate of entropy generation is stated:

$$S^*_{\text{gen}} = \frac{k}{T_0^2}(\nabla T)^2 + \frac{\mu_0}{T_0}[\mathbf{S}\nabla\mathbf{V}] \tag{30}$$

After using eq. (30), lubrication approximations and dividing the previous equation with characteristic entropy, S_{G0}, the total entropy generation number, N_G, is obtained:

$$N_G = \tau\left(\frac{\partial\theta}{\partial y}\right)^2 + \mathrm{Br}\left\{\left(\frac{\partial u}{\partial y}\right)^2 + \mathrm{We}\left(\frac{\partial u}{\partial y}\right)^3\right\} \tag{31}$$

where $\tau = \Delta T/T_0$ is the dimensionless temperature difference (we set $\tau = 1$). The first term in eq. (31) represents the irreversibility due to heat transfer and the second term signifies the fluid friction irreversibility. The average entropy generation number is calculated:

$$Ns_{\mathrm{avg}} = \frac{1}{\forall}\int_0^1\int_0^h N_G \mathrm{d}y\mathrm{d}x \tag{32}$$

where $\forall = 2$ is the area of the integrated region between $x = 0$ and $x = 1$. To see the perceptive effects of fluid friction irreversibility over the heat transfer irreversibility the Bejan number, Be, is defined:

$$\mathrm{Be} = \frac{1}{1+\Phi} \tag{33}$$

where

$$\Phi = \frac{\mathrm{Br}\left\{\left(\frac{\partial u}{\partial y}\right)^2 + \mathrm{We}\left(\frac{\partial u}{\partial y}\right)^3\right\}}{\tau\left(\frac{\partial\theta}{\partial y}\right)^2}$$

The Bejan number, is restricted between 0 and 1. The Bejan number bigger than 0.5, signifies the dominancy of heat transfer irreversibility over fluid friction irreversibility and its value smaller than 0.5 indicates that prevailing effects of fluid friction irreversibility.

Results and discussion

To discuss the effects of various parameters of interest on flow quantities, such as, axial velocity, $u(y)$, pressure rise per wavelength, ΔP, pressure gradient, $\mathrm{d}p/\mathrm{d}x$, temperature, the entropy generation number, N_G, and the Bejan number, we prepare figs. 2-22. Figures 2 and 3 reflect the effects of Hartmann number and cilia length parameter, ε, on axial velocity, $u(y)$. From fig. 2, it is seen that higher values of magnetic field parameter resist the flow in the core region of the channel and slow down fluid velocity. Whereas it accelerates the axial velocity in the vicinity of channel wall. From fig. 3 it is noticed that an increase in cilia length brings

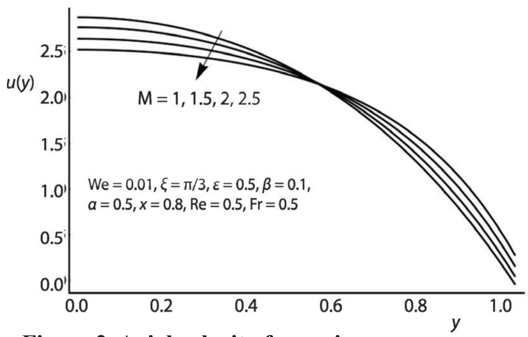

Figure 2. Axial velocity for various values of variable M

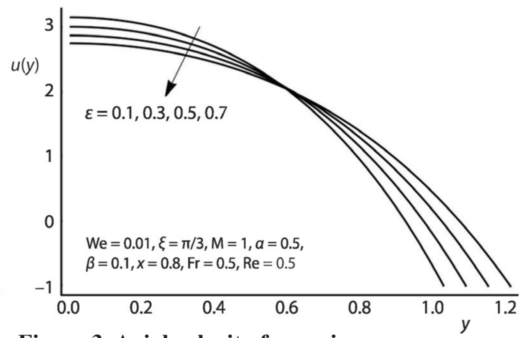

Figure 3. Axial velocity for various values of variable ε

hindrance in the core part of the channel and decelerates fluid velocity. However, the influence of cilia length at and near the channel walls is entirely opposite. Here axial velocity boosts by considering large values of cilia length parameter.

The effects of M, ε, and ξ on pressure gradient *vs.* volumetric flow rate can be anticipated through figs. 4-6. It is observed that large values of Hartmann number and ε increase pressure rise in the pumping zone but induce a decline in the augmented pumping area. It is also revealed that pressure rice is an increasing function of ξ throughout the pumping and augmented pumping regions. Figure 7 demonstrates that an increase in Hartmann number place a strong augmentation in adverse pressure gradient that may generate reverse flow. Also, this proliferation is more considerable in the core region. Figures 8 and 9 indicates that small values of cilia length ε and large values of eccentricity parameter α induce an elevation in favorable pressure gradient in the core zone of the channel as compared to its end zone.

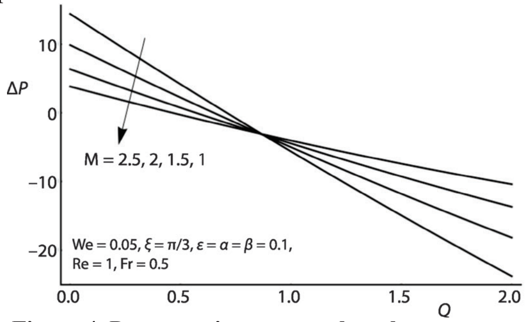

Figure 4. Pressure rise per wavelength for different values of M

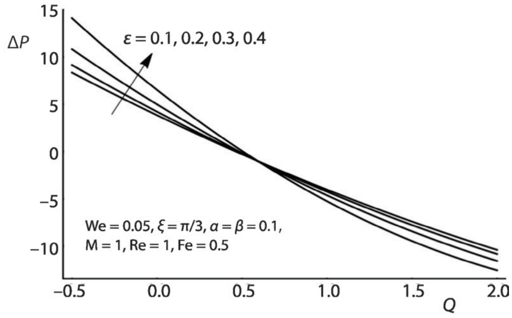

Figure 5. Pressure rise per wavelength for different values of ε

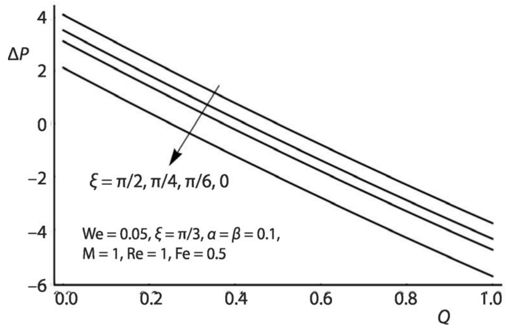

Figure 6. Pressure rise per wavelength for different values of ξ

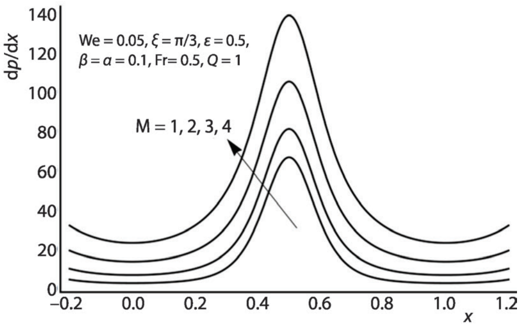

Figure 7. Pressure gradient for different values of M

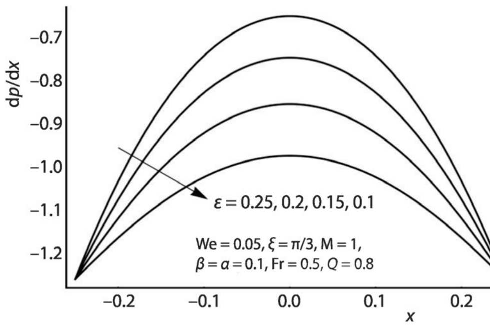

Figure 8. Pressure gradient for different values of ε

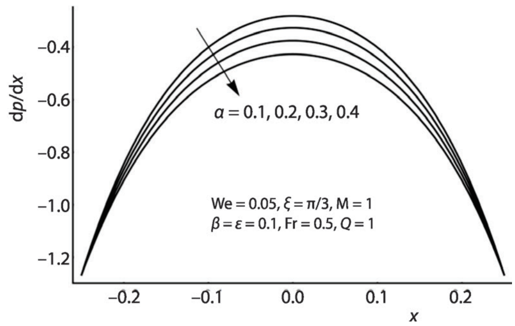

Figure 9. Pressure gradient for different values of α

Figure 10 depicts that the large values of magnetic field parameter cool down the fluid temperature. Magnetic field interprets the flow that results to bring weak convection forces and over all fluid temperature drops. Moreover, this decrease is more visible in the vicinity of channel center as compared to channel boundaries. Brink number is the measure of importance of viscous heating relative to conductive heat transfer. Figure 11 confirms that higher value of Brinkman number reduces the heat produced by viscous dissipation and hence elevates the fluid temperature. A 3-D interpretation of the temperature profile (*vs. x*- and *y*-co-ordinates) can be illustrated through fig. 12. It says that the fluid temperature is enhanced in the narrow part of the channel and is low near the wider part. This is due to presence of strong fluid fiction effects in the narrow part that tend to produce extensive internal heat generation. Figure 13 portrays a 3-D view of axial velocity. From this figure it is clear that fluid velocity is higher at the channel center than at the channel boundaries due to presence of viscous effects at the channel walls.

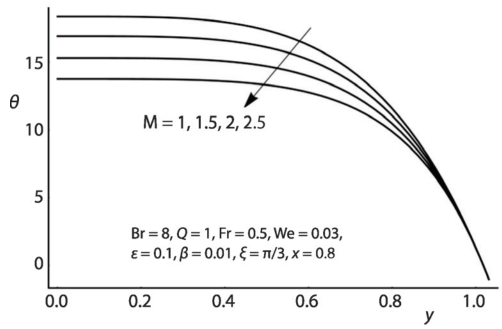

Figure 10. Temperature for different values of M

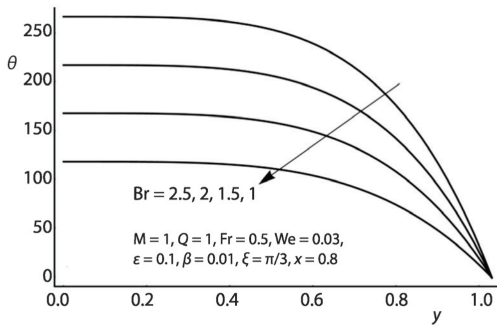

Figure 11. Temperature for different values of Br

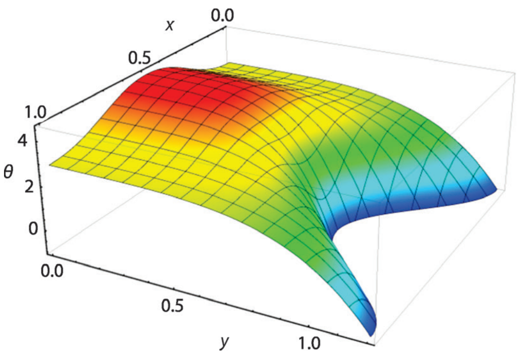

Figure 12. A 3-D view of temperature profile when M = Br = 1, α = 0.1, We = β = 0.01, ξ = π/3, Fr = 0.5

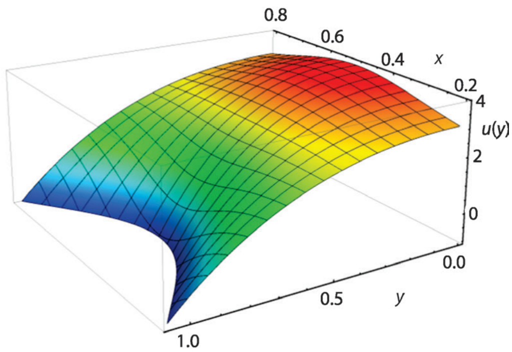

Figure 13. A 3-D view of velocity profile when M = 1, α = 0.1, We = β = 0.01, ξ = π/3, Fr = 0.5

The Bejan number plotted in figs. 14 and 15 illustrates the domination of the heat transfer effects and the fluid friction irreversibilities in the channel. It is noticed that near the channel center fluid friction irreversibility overlooks but near the heated wall irreversibility is dominated by the heat transfer effects. Moreover, Bejan nummber is observed to be a decreasing function of Hartmann number and increasing function of Brinkman number. Figure 16 validates that at the core channel zone fluid friction irreversibilities dominates and near the channel boundary, irreversibility due to heat transfer dominates. Figure 17 determines entropy generation number increases with an increase in Brinkman number. This is caused by high fluid friction effects and large heat transfer rate of poor thermal conductance of the fluids. By fig. 18,

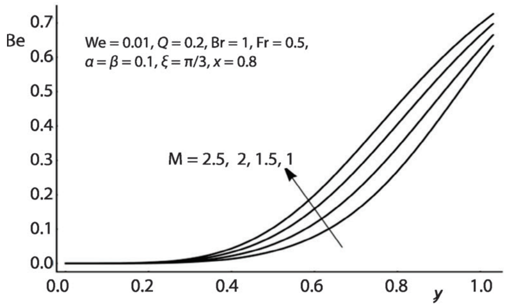

Figure 14. Effect of M on Be

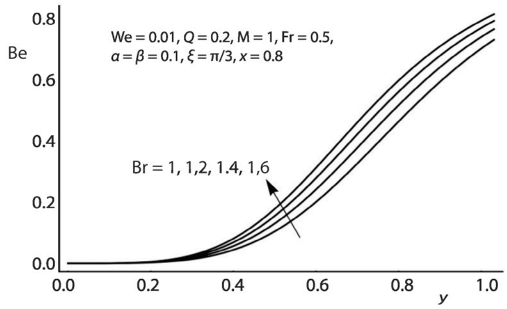

Figure 15. Effect of Br on Be

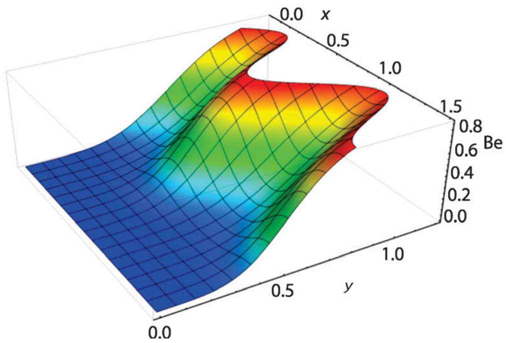

Figure 16. A 3-D view of Be when M = Br = 1, α = 0.1, We = β = 0.01, ξ = π/3, Fr = 0.5

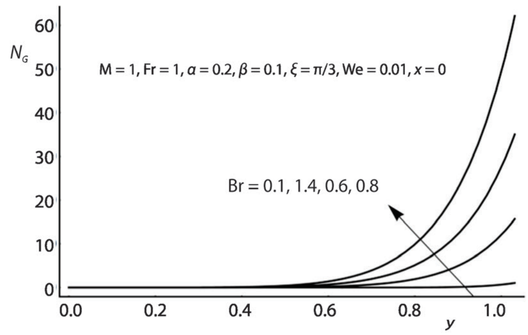

Figure 17. Effects of Br on entropy generation number

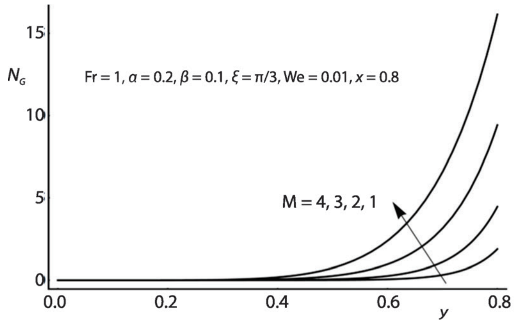

Figure 18. Effects of M on entropy generation number

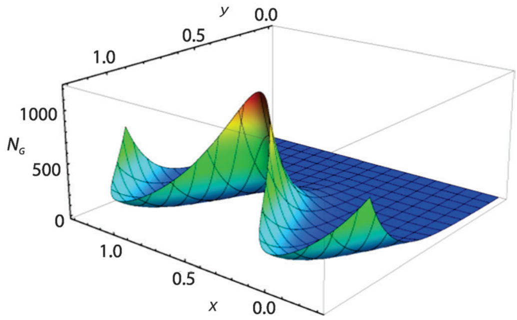

Figure 19. A 3-D view of the entropy generation number when M = Br = 1, α = 0.1, We = β = 0.01, ξ = π/3, Fr = 0.5

it is clear that high values of Hartmann number lift up the entropy generation number due to good thermal insulation of hydromagnetic fluids. A 3-D view of total entropy number against the *x*-, and *y*-co-ordinates is plotted in fig. 19. It is observed entropy is higher at the channel wall as compared to channel center. Moreover, the entropy of core region of channel is high than its edges part.

Trapping is an interesting and significant phenomenon in pumping flows. The formation of an internally circulating fluid bolus constricted by streamlines of moving metachronal waves is termed as trapping. From fig. 20, it is determined that the confined bolus reduces in size for large values of Hartmann number. Figure 21 reveals that the volume of the trapped fluid mass increases with an increase in cilia length parameter, ε. From fig. 22, it is clear that the trapped bolus decrease in size when large values of Weissenberg number are considered.

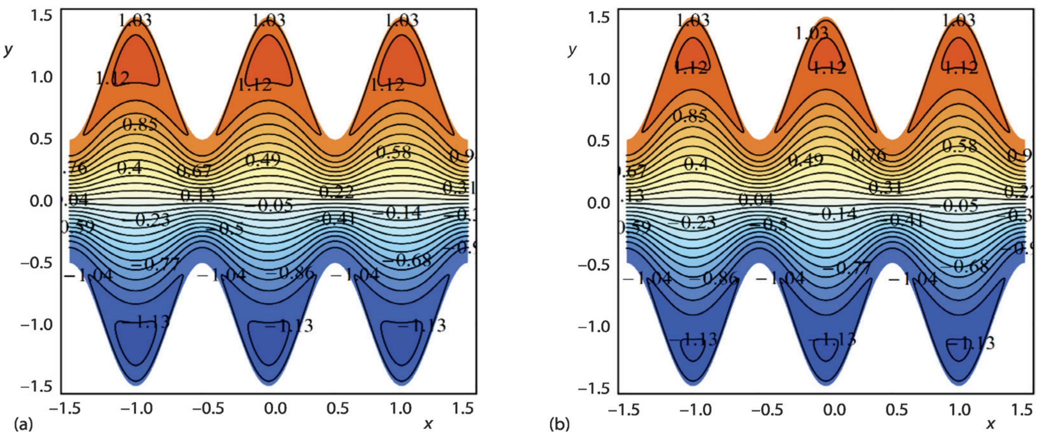

Figure 20. Streamlines for M when α = 0.2, ξ = π/3, ε = β = 0.5, Re = Fr = 1, We = 0.01; (a) M = 0.5, (b) M = 1.5

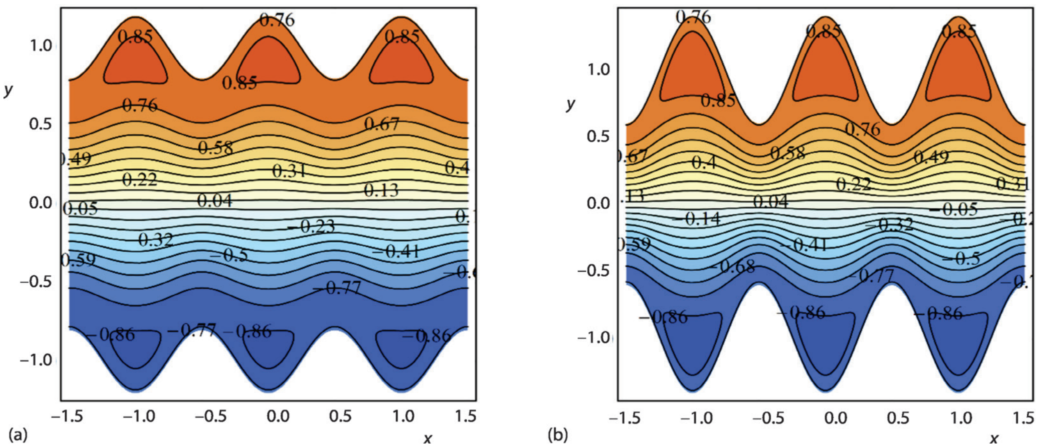

Figure 21. Streamlines for ε when α = 0.2, ξ = π/3, β = 0.5, M = Fr = Re = 1, We = 0.01; (a) ε = 0.2, (b) ε = 0.4

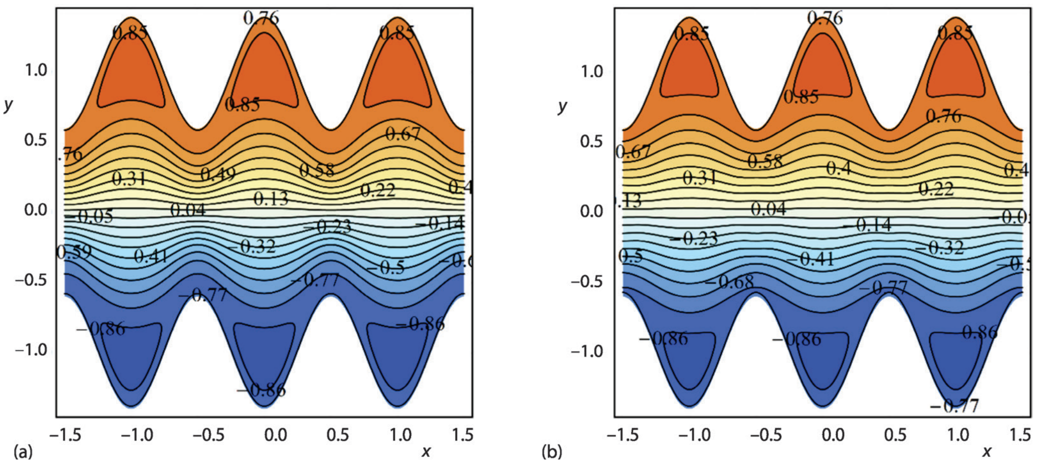

Figure 22. Streamlines for We when α = 0.2, ξ = π/3, ε = β = 0.5, Re = Fr = 1, M = 1; (a) We = 0.0, (b) We = 0.05

Conclusions

A theoretical analysis of entropy generation on pumping flow of hydromagnetic Williamson fluid is investigated in an inclined symmetric ciliated channel. The flow is induced to rhythmic (metachronal) waves of beatings of cilia. The entire study is performed in wave frame of reference. Lubrication approximations are applied on governing equations and regular perturbation method is used to solve the resulting equations. Solutions are obtained and are analyzed for various parameters of interest. The conclusion is represented in the following remarks.

- For large values of Hartmann number*,* the axial velocity decreases at the channel center and increases near the wall region.
- Higher values of cilia length parameter, ε, boost the fluid velocity at the channel walls and deaccelerate at its edges.
- The pressure rise per wavelength is an increasing (decreasing) function of Hartmann number and of cilia length parameter ε in pumping (augmented pumping) region.
- At the channel center, higher values of Hartmann number support adverse pressure gradient.
- For large values of eccentricity parameter, α, and small values of cilia length parameter, ε, favorable pressure gradient rises.
- Fluid temperature elevates when large values of Brinkman number and small values of Hartmann number are considered. Moreover, temperature is very high in in the vicinity of channel center as compared to wall zone.
- In the surrounding area of channel center, irreversibility due to fluid friction dominates. Whereas, near the channel wall, the dominancy of heat transfer irreversibility is confirmed.
- The overall entropy of the fluid increases by selecting high values of Brinkman number and small values of Hartmann number. Also, entropy of the channel increases near the wall zone as compared to channel center.
- The confined bolus decreases in size for higher values of Hartmann number and Weissenberg number. However fluid bolus enlarges when higher values of cilia length parameter ε are selected.

References

[1] Pablo, J. L., *et al*., Progress in Ciliary ion Channel Physiology, *Journal of General Physiology*, *149* (2017), 1, pp. 37-41
[2] Satir, P., Christensen, S. T., Structure and Function of Mammalian Cilia, *Histochem Cell Biol*., *129* (2008), 6, pp. 687-693
[3] Eddy, C. A., Pauerstein, C. J., Anatomy and Physiology of the Fallopian Tube, *Clinical Obstetrics and Gynecology*, *23* (1980), 4, pp. 1177-1194
[4] Gahazal, S., *et al.*, *Egg Transport and Fertilization*, The Global Library of Women's Medicine (ISSN: 1756-2228), London, UK, 2009
[5] Lehti, M. S., Sironen, A., Formation and Function of Sperm Tail Structures in Association with Sperm Motility Defects, *Biology of Reproduction*, *97* (2017), 4, pp. 522-536
[6] Wheway, G., Signaling through the Primary Cilium, *Front Cell Dev Biol*., *6* (2018), 8, pp. 1-13
[7] Brennen, C., An Oscillating-Boundary-Layer Theory for Ciliary Propulsion, *Journal Fluid Mech*., *65* (1974), 4, pp. 799-824
[8] Qiu. T., *et al*., Swimming by Reciprocal Motion at low Reynolds Number, *Nature Communications*, *5* (2014), 1, 5119
[9] Eytan, O., Elad, D., Analysis of Intra-Uterine Fluid Motion Induced by Uterine Contractions, *Bull. Math. Biol*., *61* (1999), 2, pp. 221-238
[10] Farooq, A. A., *et al*., On the Propulsion of Micropolar Fluid Inside a Channel Due to Ciliary Induced Metachronal Wave, *Appl. Math. Comput*., *347* (2019), Apr., pp. 225-235
[11] Farooq, A. A., Siddiqui, A. M., Mathematical Model for the Ciliary-Induced Transport of Seminal Liquids Through the Ductuli Efferentes, *Int. J. Biomath*., *10* (2016), 03, 1750031

[12] Ponalagusamy, R., Mathematical Analysis of Flow of Non-Newtonian Fluid Due to Metachronal Beating of Cilia in a Tube and ts Physiological Applications, *Appl. Math. Comput*., *337* (2018), C, pp. 545-561
[13] Ezzati, M., *et al*., Tubal Transport of Gametes and Embryos: A Review of Physiology and Pathophysiology, *Journal Assist Reprod Genet*., *31* (2014), 10, pp. 1337-1347
[14] Stud, V. K., *et al*., Pumping Action on Blood by a Magnetic Field, *Bull. Math. Biol*., *39* (1977), 3, pp. 385-390
[15] Maqbool, K., *et al*., Exact Solution of Cilia Induced Flow of a Jeffrey Fluid in an Inclined Tube, *Springerplus*, *5* (2016), 1, 1379
[16] Hayat, T., *et al*., Magnetohydrodynamic Flow of a Carreau Fluid in a Channel with Different Wave Forms, *Zeitschrift für Naturforschung A*, *66* (2011), 3-4, pp. 215-222
[17] Prakash, J., *et al*., Non-linear Blood Flow Analysis on MHD Peristaltic Motion of a Williamson Fluid in a Micro-Channel, *AIP Conference Proceedings*, *2112* (2019), 1, 020048
[18] Abou-Zeid, M., Homotopy Perturbation Method for MHD Non-Newtonian Nanofluid-flow through a Porous Medium in Eccentric Annuli With Peristalsis, *Thermal Science*, *21* (2017), 5, pp. 2069-2080
[19] Saleem, N. and Munawar, S., A Mathematical Analysis of MHD Blood Fow of Eyring – Powell Fluid through a Constricted Artery, *Int. J. Biomath*., *9* (2015), 02, 1650027
[20] Bejan, A., Study of Entropy Generation in Fundamental Convective Heat Transfer, *Journal Heat Transf.-Trans. ASME*, *101* (1979), 4, pp. 718-725
[21] Bejan, A., *Entropy Generation Minimization*, CRC Press, Boca Raton, Fla., USA, 1996
[22] Munawar, S., Saleem, N., Thermal Analysis of an Eyring-Powell Fluid-flow through a Constricted Channel, *Thermal Science*, *24* (2020), 2, pp. 1207-1216
[23] Mehmood, A., *et al*., Entropy Analysis in Moving Wavy Surface Boundary-Layer, *Thermal Science*, *23* (2019), 1, pp. 233-241
[24] Munawar, S., Thermal Analysis of the Flow over an Oscillatory Stretching Cylinder, *Phys. Scr*., *86* (2012), 6, 065401
[25] Souidi, F., *et al*., Entropy Generation Rate for a Peristaltic Pump, *Journal Non-Equilib. Thermodyn*., *34* (2009), 2, pp. 171-194
[26] Akbar, N. S., Entropy Generation and Energy Conversion Rate for the Peristaltic Flow in a Tube with Magnetic Field, *Energy*, *82* (2015), Mar., pp. 23-30
[27] Munawar, S., *et al*., Second-Law Analysis in the Peristaltic Flow of Variable Viscosity Fluid, *Int. J. Exergy*, *20* (2016), 2, pp. 170-185
[28] Saleem, N., Entropy Production in Peristaltic Flow of a Space Dependent Viscosity Fluid in Asymmetric Channel, *Thermal Science*, *22* (2018), 6, pp. 2909-2918
[29] Munawar, S., Saleem, N., Entropy Analysis in Cilia Driven Pumping Flow of Hyperbolic Tangent Fluid with Magnetic Field Effects, *Fluid Dyn. Res*., *52* (2020), 025503
[30] Ramesh, K., *et al*., Cilia-Assisted Hydromagnetic Pumping of Biorheological Couple Stress Fluids, *Journal Propul. Power*., *8* (2019), 3, pp. 221-233
[31] Bejan, A., Second Law Analysis in Heat Transfer, *Energy*, *5* (1980), 8-9, pp. 720-723
[32] Adesanya, S. O., Makinde, O. D., Thermodynamic Analysis for a Third Grade Fluid through a Vertical Channel with Internal Heat Generation, *Journal Hydrodyn*., *27* (2015), 2, pp. 264-272
[33] Munawar, S., Saleem, N., Entropy Analysis of an MHD Synthetic Cilia Assisted Transport in a Micro-Channel Enclosure with Velocity and Thermal Slippage Effects, *Coatings*., *10* (2020), 4, 414

Paper submitted: October 6, 2019
Paper revised: May 8, 2020
Paper accepted: May 13, 2020